

Dynamic, remote-controllable electroactive hydrogel waveguide architectures

Oscar Alejandro Herrera Cortes, Kathryn A. Benincasa, Kevin Vaughan, Derek. R. Morim, Natalie Blanchard, Tomas Omasta and Kalaichelvi Saravanamuttu*

Affiliations :

Department of Chemistry and Chemical Biology, McMaster University, 1280 Main St. West, Hamilton, Ontario L8S 4M1, Canada

*Correspondence to:

Prof. Kalaichelvi Saravanamuttu

Department of Chemistry and Chemical Biology

McMaster University

1280 Main St. West, L8S 4M1 Ontario, Canada

Email: kalai@mcmaster.ca

1 **Abstract**

2 Remote-controllable waveguide architectures inspired by living organisms with unique flexible,
3 light guiding properties were fabricated using self-trapped beams of incoherent light. Made of
4 electroactive hydrogels, light-guiding structures are generated through a nonlinear, self-inscription
5 process that utilizes visible beams from light-emitting diodes (LEDs). Due to irreversible refractive index
6 changes experienced by photoinduced chemical reactions, these self-trapped beams permanently
7 inscribe cylindrical waveguides along their paths. Taking advantage of this phenomena, we fabricate
8 macro-scale, remote controllable waveguide structures in the form of rectangular prisms and arrays of
9 cylindric waveguides. We also fabricate micro-scale structures for remote actuation, in the form of
10 rectangular prisms embedded with thousands of waveguide units. By applying and varying external
11 electric fields, we dynamically control the bending, angular orientation, and rotation (up to 360°) of these
12 pliant light-guiding structures. This allows precise, remote control of the waveguided light output.

13

14 **Main**

15 Understanding the relationship between structure and function in biological systems and
16 materials has fascinated researchers for generations.¹ The female angler fish, for example, has a
17 symbiotic relationship with a species of luminescent bacteria. This bacterium is housed within a lure that
18 dangles atop the female's head, where it has a safe environment to grow. The angler fish can direct the
19 light output of this bioluminescent species to attract prey or potential mates, by flexing this lure.^{2,3} Squid,
20 cuttlefish and octopi display remarkable camouflaging due to pigment filled organs, called
21 chromatophores, present in their skin. These organs expand upon contraction of muscle fibers when
22 triggered by an electrical stimulus. As a result, the chromatophores increase their size temporarily.⁴ The
23 visual perception by an observer is a changeable pattern in the form of an array of coloured dots that
24 seem to migrate in space, distracting the eye. Inspiration by these types of hybrid systems can lead to the
25 fabrication of stimuli-responsive, flexible, light guiding materials with remote actuation for various
26 applications.

27 Most reported soft actuators reported in the literature comprise of multi-material light guiding
28 architectures. Reminiscent to the angler fish's ability to direct light, there are currently few examples of
29 waveguide actuators reported for remote light guidance. This includes the development of liquid crystal
30 elastomer fibers patterned with gold nanoparticles,⁵ shape memory polymer fibers embedded with
31 Al₂O₃/ZnO photonic shells of varying thickness and observable structural colour,⁶ ferromagnetic soft-
32 robots embedded with optical fibers,⁷ and liquid crystal fiber arrays.⁸ Reminiscent to the visual migration
33 of chromatophores seen in squid skin, and how light can be reflected towards and away from a visual
34 observer, thermoactivated liquid crystals elastomers are able to remotely actuate and act as an optical
35 sensor. Liquid crystal elastomers undergo a transition from an opaque domain to a transparent upon
36 heating. As a result, light coupled into the transparent elastomer can then be received by a detector
37 (leading to an optical signal). The bending state of the liquid crystal elastomer translates to the amount of
38 light monitored and collected at the detector.⁹

39 3-D printing techniques that offer a fast route to create mechanically stable objects have emerged
40 in recent years. While some of them rely on sequentially depositing layers similar to the methods used in

41 traditional additive manufacturing techniques, there also exist methods capable of producing seamless
42 objects.^{10–13} Techniques that create objects employing 3D-unit operations have also emerged, such as
43 volumetric methods that rely on tomographic reconstruction^{14,15} and those that rely on the propagation of
44 nonlinear optochemical waves known as computed axial lithography (CAL).¹⁶ Objects are created by
45 launching 2D patterns calculated using the same concepts from computed tomography imaging. The
46 combined energy dose from the 2D images solidifies the resin creating the desired object.

47 Our group has demonstrated that 3D objects can be created in a single step when patterned blue
48 nonlinear beams propagate through a photopolymerizable medium.¹⁷ In traditional stereolithographic
49 methods, the thickness of the resulting film is limited to < 100 μm , due to the divergence experienced by
50 the incident beam blurring as it travels through the medium, decreasing the overall resolution. This beam
51 divergence can be controlled in nonlinear media, such as a photopolymer material, as the divergence of
52 the beam is counteracted by the photo-induced changes in refractive index originating from the
53 photopolymerization reactions. This results in the creation of 2D objects with depths > 100 μm .¹⁸
54 Additionally, these objects are homogenous along their direction of propagation since they are obtained in
55 a continuous matter without layering artifacts. Therefore, each element obtained through this method is a
56 polymer waveguide. This method can be extended to long-area waveguide lattices with large populations
57 of filaments embedded in a shape, as imposed by a 2D amplitude mask.^{19–22} This lattice would be
58 impossible to fabricate with traditional photolithographic methods, including current volumetric 3-D
59 printing techniques discussed earlier. Polymer waveguides have potential applications in light-base
60 therapies including photo-activated drug release and the migration of biological cells within a hydrogel
61 (via waveguided light).^{23,24}

62 Herein, we describe the fabrication and demonstration of different geometries of flexible, light
63 guiding structures as inspired by deep sea creatures. These geometries include a planar rectangular
64 prism; individual and small arrays of cylindrical waveguides; and a rectangular prism embedded with long-
65 range micro-scale waveguide filaments. Using a stimuli-responsive electroactive hydrogel, we have
66 demonstrated that the fabricated waveguides motion and orientation can be precisely and remotely
67 controlled through external electrical fields. Reminiscent of the bioluminescent lure directed by the female
68 angler fish to attract prey, we demonstrate how a flexible electroactive waveguide's light output can be

69 precisely controlled due to the degree of bending experienced by the waveguide, and how the light output
70 is successfully directed to and from a detector. Reminiscent of chromatophores found in various
71 cephalopods and how the arrays of pigment migrate in space to distract predators, we demonstrate how
72 micro-lattices of waveguides display a similar behaviour, guiding their light output as a bright array of dots
73 in space to a detector.

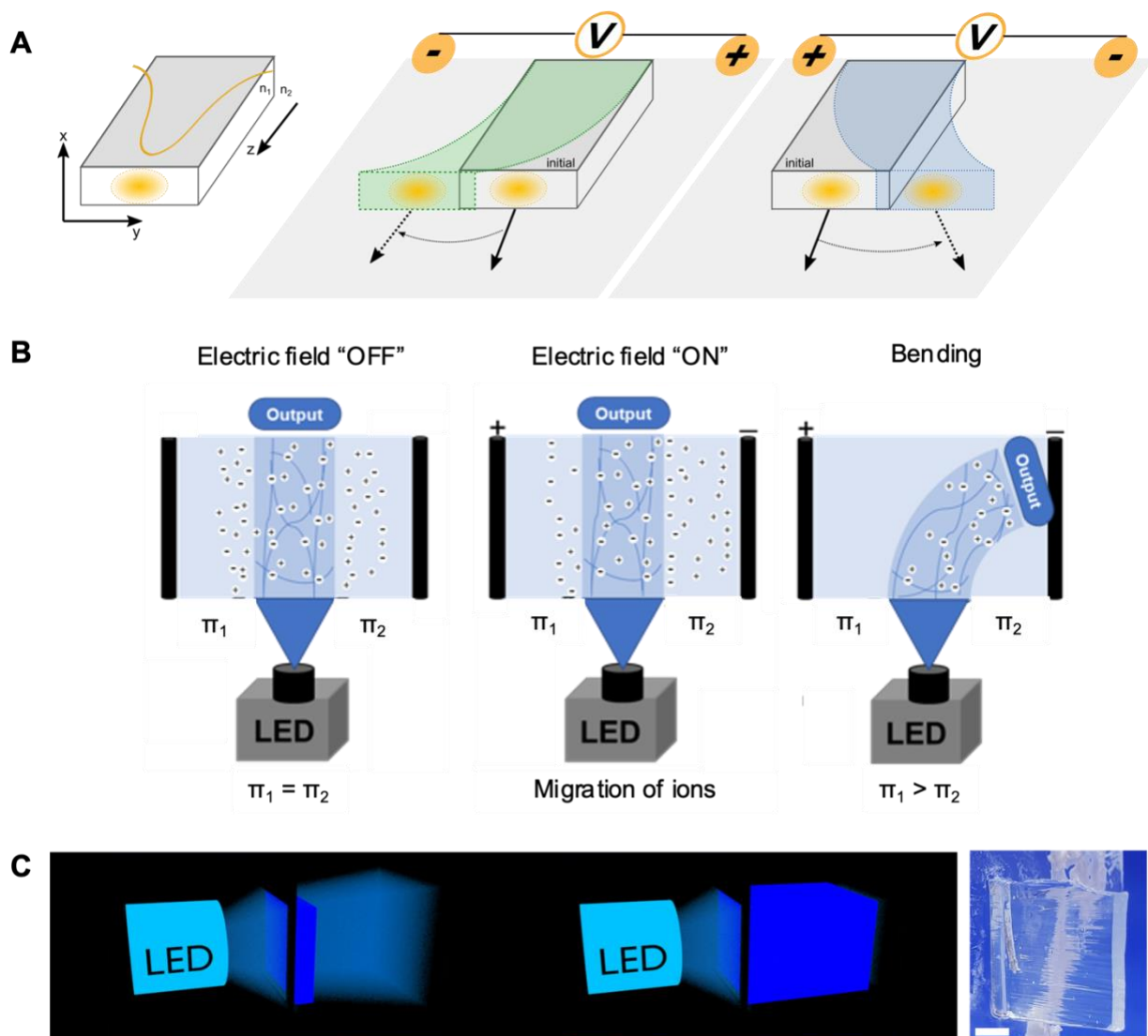
74 Through the vectorial sum of external electric fields, we can dynamically control the bending,
75 angular orientation, and rotation (up to 360°) of these flexible, light-guiding structures. This allows for
76 precise, remote control of the waveguided light output without the use of computers or other electronic
77 devices. Flexible fiber-like structures that decrease their brightness while bending can act as sensors in
78 prosthetic hands or artificial skins.^{25,26} Additionally, fabricating stimuli-responsive waveguides or actuators
79 with waveguide-circuitry embedded can help to develop highly sophisticated soft robots that can detect
80 their own shape or deformation state.^{27,28} They could also become part of devices that can be used for
81 minimally invasive surgery or light-based therapies.²⁹

82

83 Unidirectional actuation of hydrogel waveguides

84 An optical waveguide is a dielectric structure that can guide electromagnetic waves. Guided
85 waves are dependent on the phenomenon of total internal reflection (TIR), which confines light to travel
86 along the optical axis of a waveguide. The core region of a waveguide is assumed to have a refractive
87 index (n_1) higher than the surrounding material (n_2) to achieve TIR (**Figure 1a**, left).³⁰ The material
88 presented herein is a flexible, electroactive hydrogel. This means that as an electric field is applied the
89 flexible waveguide will bend in the direction of the cathode, continuing to guide light along its optical axis
90 (**Figure 1a**, center). This light will be guided to a detector (i.e., CCD camera) and will continue to be
91 collected so long as the waveguided light is within the detectors field of view, or light collection range. If
92 the polarity of the electric field is inverted, the waveguide will bend the opposite way continuing to guide
93 light as it moves (**Figure 1a**, right). The bending of the hydrogel is caused by the flow of ions in solution
94 as they migrate through the porous hydrogel to the cathode. This is a direct result of the material used to
95 fabricate the waveguide structures.

96 Hydrogel resin used to fabricate planar waveguides was developed using two previously
97 described formulations.^{31,32} The precursor, denoted as **H1** (see **Methods and Materials 5.1** for resin
98 formulation), consists of acrylic acid, N,N'-methylenebis(acrylamide) crosslinker, Irgacure® 819 ($\lambda_{\text{max}} =$
99 468 nm) photoinitiator and sodium phosphate buffer solution (pH = 7.4). Although there is buffer present
100 in the resulting hydrogel, only $\approx 2\%$ of monomers are deprotonated after fabrication. When the hydrogel
101 is immersed in buffer solution, most acrylic acid monomers lose their acidic proton producing an anionic
102 network (**Figure 1b**, left). When an electric field is applied, the counterions within the hydrogel bound to a
103 carboxylate group remain within the network to preserve the electroneutrality inside the gel. Counterions
104 that are not bound migrate freely in the solution and within the gel towards the cathode. The migration of
105 negative ions within the gel is hindered since the network is negatively charged. As a result, there is a
106 higher concentration of ions on the cathode side than in the anode side (**Figure 1b**, center). This
107 concentration gradient generates a higher osmotic pressure on the anode side (π_1 ; swelling) than on the
108 cathode side (π_2 ; shrinkage).^{33,34} The pressure difference, $\pi_1 > \pi_2$, causes bending of the gel (**Figure 1b**,
109 right) toward the cathode.



110

111 **Figure 1 | Electroactive waveguide working principles. a)** Scheme depicting a rectangular waveguide
 112 (refractive index, n_1) guiding an optical mode to the entrance face of the waveguide (represented by the
 113 yellow circle) through TIR. In the presence of an electric field, the waveguide bends moving to a new
 114 position while still guiding light. **b)** Scheme of bending mechanism in electroactive hydrogels. Changes in
 115 osmotic pressure ($\pi_1 > \pi_2$) result in bending. **c)** Scheme depicting the self-inscription process of
 116 rectangular waveguides obtained by launching a blue LED beam through a rectangular shape mask. The
 117 resultant waveguide generated through photopolymerization of **H1** precursor is shown on the right. (scale
 118 bar = 2 mm)

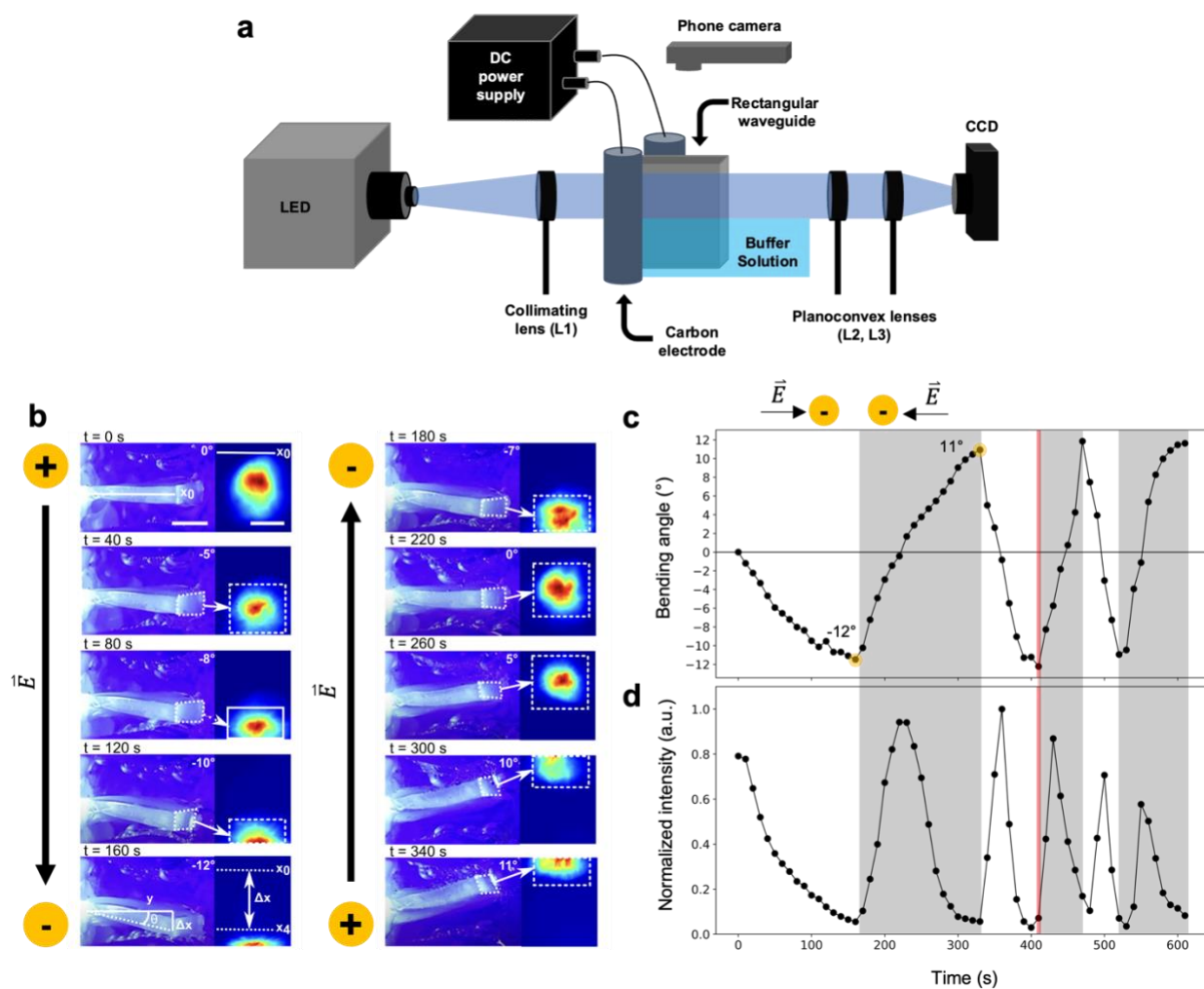
119 Rectangular hydrogel waveguides were obtained by launching a blue ($\lambda = 445$ nm) LED beam
 120 through a rectangular shape mask (**Figure 1c**, left) pasted to a glass coverslip. Free-radical
 121 polymerization of acrylic acid monomers were initiated launching these patterned beams to cells
 122 containing the **H1** hydrogel precursor. The refractive index change initiated by the photopolymerization
 123 reaction counteracts the natural diffraction of light, allowing the patterned beam to travel without diverging

124 **(Figure 1c**, middle) while inscribing a polymeric structure (**Figure 1c**, right). These rectangular prisms
125 remained on the coverslip (with shape mask removed), acting as the entrance face of the cell in which
126 they were fabricated.

127 To investigate the remote actuation of these hydrogel structures, a rectangular waveguide
128 adhered to a glass coverslip was placed between two carbon electrodes (placed 7 mm apart) and partially
129 immersed in a phosphate buffer solution (pH = 7.4). A blue ($\lambda = 445$ nm) LED beam was collimated and
130 launched through the part of the waveguide that was not immersed in the buffer solution. The beam
131 output of the waveguide was monitored with a CCD camera while the position of the waveguide was
132 tracked using a cellphone camera (**Figure 2a**). With an electric field applied, the waveguide bends
133 towards the cathode and the beam output shifts in the same direction. This demonstrates how light
134 confined within the prism can be spatially manipulated. (**Figure 2b**).

135 The polarity of the electric field was inverted when the monitored intensity output for the planar
136 waveguide reached a steady, nonchanging value (roughly 60 s). When the polarity of the electric field
137 was inverted, the bending direction reverses as a result (**Figure 2b** and **video S1**). The maximum
138 bending angle for rectangular waveguides 10 mm long is calculated to be -12° (see **Supplementary**
139 **Information S1** and **Figure S1** for the calculation of bending angle). This was achieved at 410 s, after
140 which the electric field had been inverted twice (**Figure 2c**). As expected, there is a noticeable drop in the
141 intensity when bending angles begin to approach a local maximum. This is due to confined light within the
142 waveguide being directed away from the detector (i.e., CCD camera). The net effect every time the
143 waveguide reaches the maximum bending angle, or similarly large angle, is a bright sheet (with ≈ 2 mm
144 thickness) that seems to turn “off” from the point of the observer or detector. Quantitatively, this directly
145 translates to the intensity output of the waveguide decreasing by $\approx 90\%$ on average (**Figure 2d**). The
146 intensity of the beam is recovered when the waveguide is perpendicular to the detector or reaches a
147 bending angle of $\theta \approx 0^\circ$. For the waveguides 6 and 9 mm long the maximum bending angle is $\approx -2^\circ$ and \approx
148 -11° , respectively. When these bending angles are reached, the intensity of the beam output decreases to
149 ≈ 22 and $\approx 75\%$ of its original value, respectively. Graphs showing the time evolution of bending angle
150 and beam output intensity of these waveguides can be found in **Figure S2**.

151 In the experiment shown in **Figure 2c**, the rectangular waveguide is able to reach maximum
 152 bending angles faster after the electric field has been applied in two actuations (i.e., after 300 s), than
 153 compared to the beginning of the experiment. This is most likely caused by an increase of fixed charge
 154 density in the network (mole fraction of charged species) as the hydrogel swells and more carboxylic acid
 155 groups get deprotonated. It has been previously shown, in hydrogels with acrylic acid as the monomeric
 156 unit, that the rate of bending increases with the fixed charge density if the total charge density is below
 157 70%.^{32,35}



158
 159 **Figure 2 | Remote actuation of a planar, hydrogel waveguide.** **a)** Optical setup used for the electro-
 160 actuation of rectangular hydrogel waveguides. Light from a blue LED was collimated (L1, f.l. = 250 mm)
 161 and launched to the entrance face of the waveguide. Imaging of the optical profile at the exit face of the
 162 waveguide was achieved using a pair of a planoconvex lenses (L2, L3, f.l. = 250 mm) and a high-
 163 resolution charge-coupled device (CCD) camera. A phone camera captured the top-view actuation of the
 164 gel. **b)** Top-view waveguide actuation (scale bar = 4 mm) with complimentary 2D beam intensity profiles
 165 (scale bar = 1 mm) of a waveguide 10 mm long under the effect of an electric field (1300 V/m) when

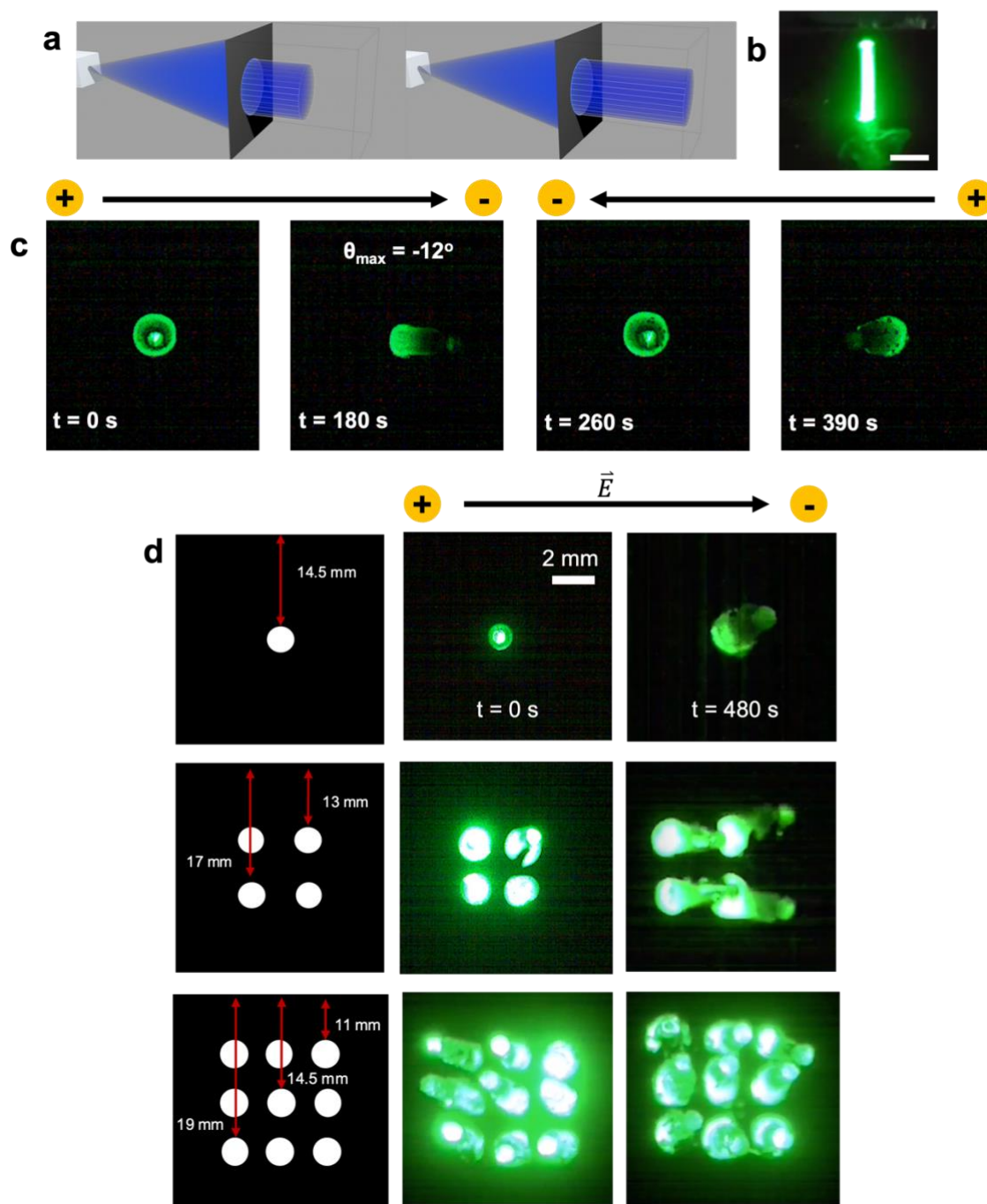
166 irradiated with a blue LED (see **video S1**). **c**) Time evolution of the bending angle as the electric field is
167 applied. The maximum bending angle (-12°) is indicated by a red line on the graph. Electric field polarity
168 inversions are indicated above the graph. **d**) Normalized intensity of the beam output of the waveguide as
169 the electric field is applied. As the waveguide bends away from the optical set up, the intensity on the
170 detector decreases $\approx 90\%$ when the maximum bending angle is reached (as indicated by the red line).

171 The method of hydrogel fabrication is widely versatile to different shapes and architectures of light
172 guiding geometries. To demonstrate this versatility, cylindrical hydrogel waveguides were fabricated using
173 a blue LED ($\lambda = 445 \text{ nm}$) launched through a circular shape mask (**Figure 3a**) placed at the entrance face
174 of a cell containing hydrogel precursor **H1**. The fabricated cylindrical waveguide was kept vertical for the
175 following unidirectional remote actuation investigations (**Figure 3b**). A scheme of the setup used for these
176 experiments is shown in **Figure S3**, which consists of a power supply connected to rectangular carbon
177 electrodes inserted on the sides of a custom 3D printed cage. In the middle of the cage is a hole in which
178 a 10 mm cylindrical hydrogel waveguide can be placed. Sodium phosphate buffer (pH = 7.4) solution
179 covered around 8 mm ($\approx 80\%$) of the cylindrical waveguide, with the remaining top portion exposed to air.
180 While an electric field was applied to actuate the cylinder, an attenuated beam from a compact laser
181 module ($\lambda = 520 \text{ nm}$) was launched through the bottom. The spatial evolution of the cylinder and the
182 intensity of its beam output was recorded using a Moticam 3+ CMOS camera (**Figure 3c**).

183 To observe the unidirectional motion of the hydrogel cylinder, the polarity of the applied electric
184 field was inverted every 180 s. A maximum bending angle of -12° was achieved at 180 s, at the end of the
185 first actuation. After applying the electric field for roughly 400 s (i.e., two electric field actuations), the
186 intensity of the outputted beam starts to decrease over time. This is a result of three factors: fatigue
187 damage; the fracture plane created near the base of the hydrogel when the cylinder bends and/or swells;
188 and droplets of water containing carbon particles (from the carbon electrodes) built up on the waveguide
189 tip over time, consequently blocking the beam output. As a result of these factors the intensity we can
190 visually see the beam fully recover at $\approx 260 \text{ s}$, as the waveguide points directly at the camera again (i.e.,
191 $\theta \approx 0^\circ$) (see **video S2** for the entire recorded experiment).

192 Unidirectional actuation of square arrays of four (2×2) and nine (3×3) cylindrical waveguides
193 were also demonstrated. To actuate cylindrical arrays of waveguides vertically, a similar setup was used
194 as described in **Figure S3a**. The only difference presented here is the presence of additional holes in the
195 base of the cage to accommodate for the additional cylindrical waveguides (**Figure 3d**). Arrays of

196 waveguides were illuminated and actuated in a unidirectional fashion. A general trend can be observed
197 for both rectangular and cylindric waveguide unidirectional remote actuation, with respect to light
198 guidance and control. When the electric field is applied, the waveguide in question bends towards the
199 cathode and the intensity of the beam output decreases as the light output is guided away from the
200 detector. This trend is also observed when the polarity is reversed and the waveguide bends in the
201 opposite direction. The light intensity can be fully regained once the waveguide is aligned again with the
202 detector, thus the light output is guided towards it and is recovered.



203

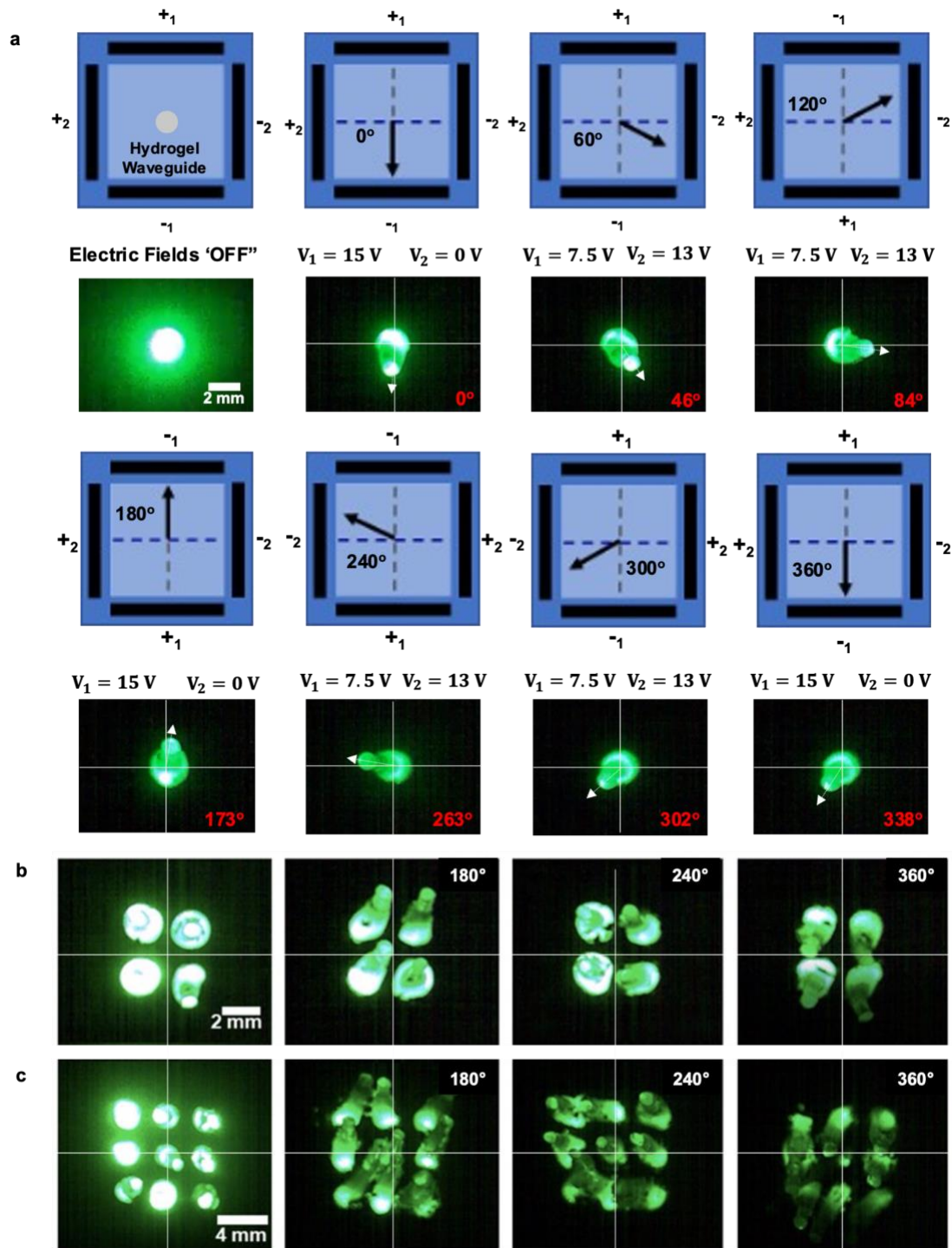
204 **Figure 3 | Vertical remote actuation of cylindrical hydrogel waveguide.** a) Fabrication scheme for the
 205 cylindrical hydrogel waveguides. Light from a blue LED is launched through a circular shape mask, to the
 206 **H1** precursor. b) Image of the cylindric waveguide when illuminated with a green laser beam (scale bar =
 207 5 mm). c) Time evolution images of a cylindric waveguide under the effect of an electric field (520 V/m)
 208 (see **video S2**). Electric field polarity switches are as indicated. d) Scheme of cages used to house
 209 cylindric waveguide arrays, highlighting the distance away from the cathode each cylinder was based on
 210 the cage and array implemented. Cylindric waveguides are irradiated with an expanded green beam ($\lambda =$
 211 520 nm) and actuated with an electric field (520 V/cm) (see **video S3**).

212

213 **Multidirectional actuation of arrays of cylindric waveguides**

214 Most actuation of electroactive hydrogel structures involves unidirectional bending and
215 locomotion with a single pair of electrodes.^{32,35} Upward propulsion can also be achieved with a single pair
216 of electrodes by applying alternating electric fields, which was demonstrated by Zhao et al.³⁶ Here the
217 authors designed an electroactive hydrogel, which had four “tentacles”, inspired by jellyfish movements.
218 Bending the tentacles upwards using a voltage of 7 V followed by a downward realignment by applying a
219 higher voltage (15 V) in the opposite direction produced an upward propulsion. Using arrays of four
220 electrodes has been proven to be an efficient way to achieve complex motions in electroactive hydrogel
221 structures. This approach has also been applied to ionic polymer metal composites by placing electrodes
222 on orthogonal positions of the polymer surface,^{37,38} where bending is limited to 90° and 45°.

223 We have demonstrated arrays of cylindric waveguides can be unidirectionally actuated with the
224 application of a single electric field. By combining two electric fields through vectorial analysis (**Figure**
225 **S3b** and **Figure S3c** for vectorial analysis used for the following investigations), arrays of cylindric
226 waveguides can be remotely bent, precisely, in multiple directions. To accomplish this, the combined
227 electric field was kept constant (520 V/m) to achieve targets angles of: 0°, 60°, 120°, 180°, 240°, 300° and
228 360°. Bending angles for the following experiments were calculated only for the individual cylindric
229 waveguide placed in the center of the square array (**Figure 4a**). We used the first bending direction of the
230 cylinder as a reference point (i.e., $\theta = 0^\circ$). For the initial bending direction, the electric field was applied for
231 240 s, after which it was applied for 180 s for each direction after. This process was repeated until
232 cylindrical waveguides completed a full cycle (see **video S4** for single and arrays of waveguides rotating).
233 Experimental bending angles for the individual waveguide were calculated to be: 0°, 46°, 84°, 173°, 263°,
234 302° and 338° (as indicated in **Figure 4a**). While the calculated experimental angles show some deviation
235 from the target angles, this approach allows precise control over the waveguide’s direction, thereby
236 allowing for multidirectional rotation of the waveguide. The intensity of the waveguide output remains
237 steady as it bends, initially. Over time the intensity output begins to decrease, which can be attributed to
238 damage experienced by the hydrogel. The same combined electric field was also applied for each
239 configuration of cylindric waveguide arrays; (2 x 2) (**Figure 4b**) and (3 x 3) (**Figure 4c**).



240

241 **Figure 4 | Multidirectional bending of cylindric waveguide arrays.** **a)** Configurations used to direct the
 242 cylindric waveguide. Target angles are displayed along with the electric field vectors used to orient the
 243 waveguide. Experimental images of each output displayed below, with calculated bending angles (red)
 244 displayed alongside each image. **b)** 2x2 and **c)** 3x3 cylindrical waveguide array experimental output.
 245 Target angles (white) displayed alongside images.

246

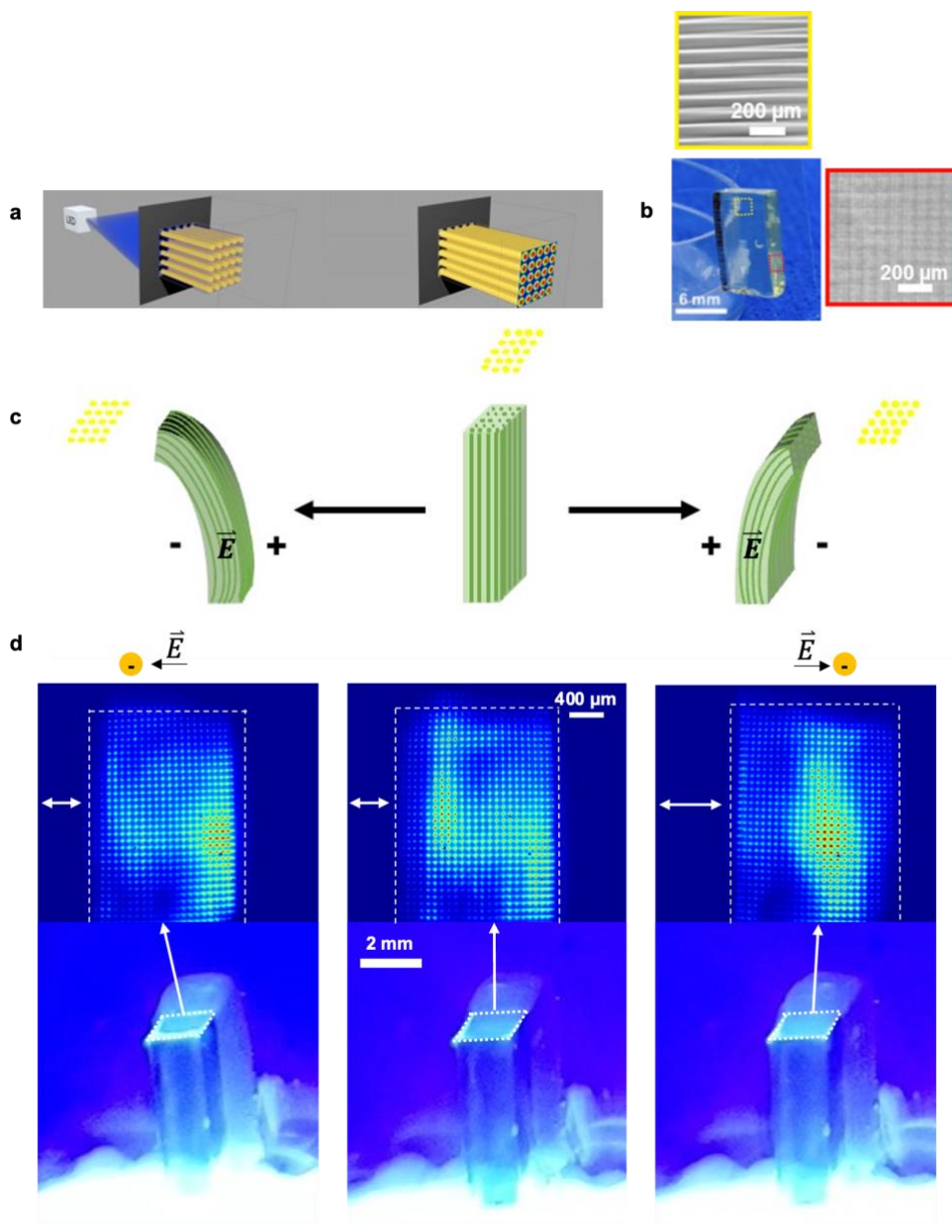
247 **Unidirectional remote actuation of a micro-waveguide array**

248 We have previously shown that it is possible to fabricate micro-waveguide arrays in an
249 organosiloxane photopolymer.³⁹ We hypothesize that creating these arrays using an electroactive
250 hydrogel would allow the formation of a structure with a bright array of dots that would seem to migrate in
251 space from the point of view of an observer, reminiscent of the chromatophores seen in various types of
252 cephalopods which present as dots migrating in space. Like the behaviour observed in the planar and
253 cylindric hydrogel waveguides, light traveling through these waveguide micro-channels will be confined
254 and guided towards the direction in which the waveguide is bending.

255 To explore this, waveguide lattices were inscribed within hydrogel prisms ($L = 6$ mm, $W = 2.5$
256 mm). The hydrogel precursor used to fabricate waveguide lattices was similar to precursor **H1**, with the
257 added use of camphorquinone (CQ) co-initiator. This adapted precursor is hence denoted as **H2**. The
258 inclusion of CQ as a co-initiator in the photoinitiated free radical reaction will produce a lower
259 concentration of free radicals, thereby resulting in a smaller degree of polymerization.⁴³ This will produce
260 the refractive index contrast needed for the formation of prisms with waveguides embedded. To fabricate
261 hydrogel micro-lattices, the process to create rectangular waveguides was repeated, with the addition of a
262 periodic amplitude mask ($\Lambda = 80$ μm) used to order the emerging periodic microstructure (**Figure 5a**).
263 When examined through transmission optical microscopy, an array of waveguides can be seen in the
264 longitudinal axis and along the axis of light propagation (**Figure 5b**).

265 When an electric field is applied to the hydrogel, the micro-lattice will bend according to the
266 polarity of the applied field, therefore directing the light guided by the embedded waveguides (**Figure 5c**).
267 This is seen experimentally, when a blue LED ($\lambda = 445$ nm) launched into one end of the hydrogel (at low
268 intensities) shows the presence of an array of bright micro-beams with non-uniform intensity and with the
269 same periodicity of the amplitude mask used to create the pattern (**Figure 5d**, middle). Under the effect of
270 an electric field the waveguide bends towards the cathode while the array of micro-beams also moves in
271 the same direction (**Figure 5d**, left) (see **video S5**). Changing the polarity of the electric field after 100 s
272 produces the same effect, now in the opposite direction (**Figure 5d**, right). The ability of the structure to
273 direct light in the same direction of the bending is evident when looking at the zoomed areas at the top of

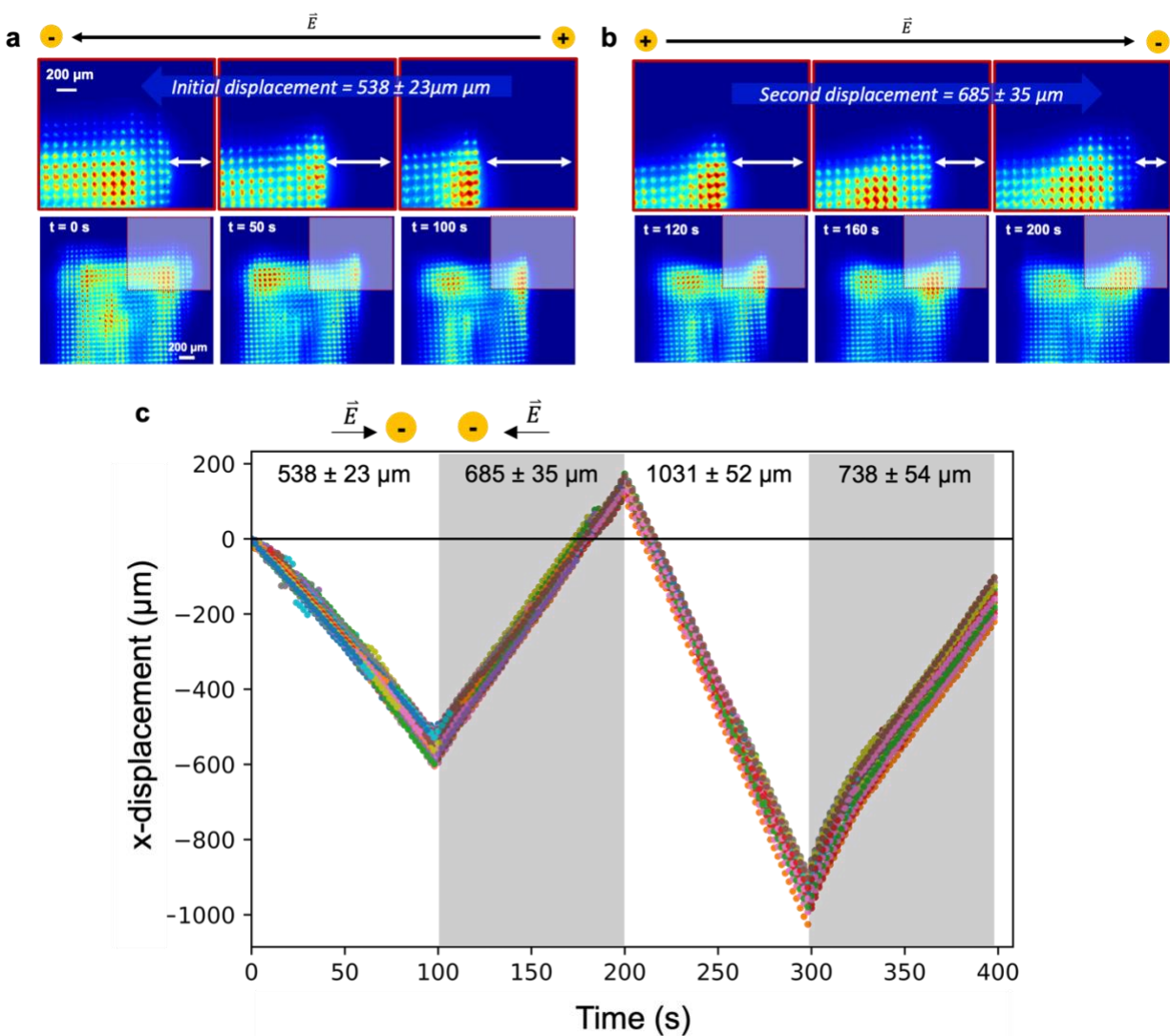
274 each of the CCD images. This is further confirmed qualitatively when the light pattern coming out of the
 275 lattice is projected onto a black surface, in conjunction with a compact laser module light source ($\lambda = 635$
 276 nm) (see **video S6**).



277
 278 **Figure 5 | Remote actuation of the hydrogel micro-lattice.** **a)** Fabrication of the hydrogel micro-lattice
 279 using a periodic amplitude mask. **b)** Transmission optical micrographs of hydrogel micro-lattice (H x L x W
 280 = 10 mm x 6 mm x 2.5 mm), with coloured regions highlighting areas of optical imaging. **c)** Bending
 281 scheme of hydrogel prism demonstrating light output based on electric field polarity (as indicated). **d)**
 282 Time evolution of the hydrogel waveguide lattice under the effect of an electric field (350 V/cm). The
 283 electric field was applied for 100 s, before inverting to reverse the direction of the micro-lattice. The
 284 square light pattern generated by the lattice moves towards the cathode (see **video S5**).

285 Positions of waveguides within the hydrogel lattice were analyzed using Trackpy,⁴⁰ a Python
286 particle tracking package (see **Supplementary Information S4** for details regarding this program). Data
287 and image sets were collected by applying an electric field for 100 s in one direction (**Figure 6a**), before
288 inverting the electric field polarity (**Figure 6b**). Waveguide light output was detected using CCD camera
289 images, where most of the waveguide trajectories (“tracks”) can be quantified as measured
290 displacements. In the first 100 s (before the electric field polarity is reversed), the whole pattern is initially
291 displaced $538 \pm 23 \mu\text{m}$ (**Figure 6a**). After that, the electric field is turned off for 60 s to allow the hydrogel
292 micro-lattice to stabilize, and consequently allow the light output reaching the detector to steady. This
293 pattern of applying the electric field for 100 s before allowing the gel to rest for 60 s is repeated for the
294 rest of the experiment.

295 The largest overall displacement experienced by the gel is $1031 \pm 52 \mu\text{m}$. This is explained by
296 qualitative swelling experienced by the gel as the experiment progresses, resulting in a more flexible
297 hydrogel. When comparing the movement of all the filaments together (**Figure 6c**), a concerted pattern
298 emerges. The intensity output of the waveguides in the micro-lattice demonstrates a completely different
299 behavior compared to the intensity output of the rectangular and cylindrical waveguides. Unlike these
300 waveguides, which demonstrate intensity decreases and recovery as light output is directed away and
301 towards a detector (i.e., CCD camera), the intensity output of the micro-lattice shows random fluctuations
302 which indicate complex dynamics taking place within the lattice (**Figure S4d**).



303

304 **Figure 6 | Quantification of individual waveguide displacement within the hydrogel micro-lattice. a)**
 305 CCD images demonstrating the hydrogel micro-lattice moving toward the cathode. The average x-
 306 displacement in this initial actuation (i.e., $t = 0-100$ s) is $538 \pm 23 \mu\text{m}$. **b)** After reversing the polarity of the
 307 electric field, the hydrogel micro-lattice moves in the opposite direction resulting in a x-displacement of
 308 $683 \pm 35 \mu\text{m}$ ($t = 100 - 200$ s). **c)** Graph overlaying all trackable waveguide filaments x-displacements.
 309 The average x-displacement is indicated when the electric field polarity is reversed.

310 Conclusions

311 Taking inspiration from the properties of living organisms – such as the bioluminescent lure of the
 312 female angler fish and chromatophores of squid skin – we have fabricated remote controllable
 313 electroactive hydrogel waveguides for precise light control and guidance. We have demonstrated that
 314 their orientation, motion and thereby direction of waveguided light can be remotely controlled using
 315 electric fields. As the method of fabrication is not restricted by the photopolymer used, this results in a

316 large range of versatility in the light guiding structures produced. Therefore, this work also pathways to
317 fabricate not only electroactive waveguide actuators in a single step but also thermal⁴¹ or
318 photoresponsive waveguides⁴² that can respond to more than one stimulus.

319 **Acknowledgements**

320 We thank the Moran-Mirabel research group and Lyons Media Center at McMaster University for
321 access to instrumentation. We also thank Marcus Rose for his guidance in designing the initial stages of
322 image processing for the Trackpy program. We thank Ciba-Geigy for the generous donation of the
323 photoinitiator, Irgacure ® 819. Funding from the Natural Sciences and Engineering Research Council,
324 Canadian Foundation for Innovation and McMaster University is gratefully acknowledged.

325 **Methods**

326 **Hydrogel resin formulation**

327 The hydrogel precursor **H1** was used for planar and cylindrical waveguides. **H1** was obtained by
328 mixing 67.61 mmol of acrylic acid (Sigma Aldrich, Canada), 6.94 mmol of N,N'-methylenebis(acrylamide)
329 (Sigma Aldrich, Canada) as crosslinker, 4.48×10^{-2} mmol of Irgacure ® 819 (Ciba Specialty Chemicals)
330 as photoinitiator and 5 mL of sodium phosphate buffer solution 0.4 M (pH = 7.4). The hydrogel precursor,
331 **H2**, used to fabricate hydrogel prisms patterned with waveguide channels was a slightly modified version
332 of **H1** precursor. In this case, Irgacure ® 819 (2.24×10^{-2} mmol) was used in combination with 1.20×10^{-2}
333 mmol camphorquinone (Sigma Aldrich, Canada).

334 **Fabricating hydrogel waveguides**

335 Waveguides were fabricated by launching a blue LED ($\lambda = 445$ nm, Thorlabs, $I \approx 0.94$ mW mm⁻²)
336 beam through a rectangular shape mask placed at the entrance face of cells containing hydrogel
337 precursor **H1** (**Figure 1c**). The beam propagated through cells with transparent coverslips as exit and
338 entrance face with pathlengths (L) of 6, 9, and 10 mm ($W \times H = 2$ mm \times 10 mm), for 14 - 20 s, while
339 triggering localized free radical polymerization. The beam was blocked when the polymeric waveguide
340 reached the exit face of the cell. Once the process was completed, the coverslip at the entrance face was
341 removed with the polymer structure still attached. This procedure was followed to fabricate cylindric

342 waveguides with pathlength of 10 mm (**Figure 3c**), with the change of a circular shape mask used in
343 place of a rectangular one.

344 To obtain rectangular prisms embedded with micro-waveguides, a blue LED ($\lambda = 445$ nm,
345 Thorlabs, $I \approx 0.94$ mW mm⁻²) beam was collimated using a planoconvex lens (f.l. = 250 mm). The
346 collimated beam was passed through a 2D periodic amplitude mask ($\Lambda = 80$ μ m, Photomask PORTAL)
347 before being launched through a rectangular shape mask that defined the shape of the prism (H x L x W
348 = 10 mm x 6 mm x 2.5 mm), containing hydrogel precursor **H2** (**Figure 6a**). All micro-patterned prisms
349 were irradiated for 12 s.

350 **Unidirectional remote actuation of rectangular hydrogel waveguides**

351 Fabricated rectangular prism waveguides were used immediately without any further treatment as
352 they began to lose optical transparency upon swelling, becoming more brittle as their swelling ratio
353 increased. Waveguides (W x H = 2 mm x 10 mm) 6, 9 and 10 mm long were glued to coverslips between
354 two graphite electrodes (placed 7 mm apart). Once the cylinder was adhered to a cover slip, this unit was
355 glued in place within a 3D printed rectangular cage that had sides sealed with glass coverslips.

356 Waveguides were partially immersed in a phosphate buffer solution (pH = 7.4, 0.4 M) that acted
357 as an electrolyte solution. A blue LED ($\lambda = 447$ nm, Thorlabs) beam was first collimated (L1; f.l. = 250
358 mm) before being launched through the top part of the waveguide not immersed in the buffer solution.
359 Imaging of the optical profile at the exit face of the gel was achieved with a planoconvex lens pair (L2, L3;
360 f.l. = 250 mm) and a high-resolution charge-coupled device (CCD) camera (1200 (H) x 1024 (V) pixels;
361 pixel size = 3.2 μ m horizontal x 3.2 μ m). Integrated intensities were obtained by adding the intensity of all
362 the pixels in each image, which were then normalized to the maximum value. The bending of the hydrogel
363 was monitored with a cellphone camera (Samsung Galaxy 9) placed at the top of the electrochemical cell.
364 A DC power supply (BK1735A-ND, B&K Precision) was used to generate the electric field. The polarity of
365 the electric field was inverted when the monitored intensity output for the planar waveguide reached a
366 steady, nonchanging value. This process was repeated until fatigue damaged in the hydrogel was
367 observed.

368 To actuate micro-patterned prisms the same assembly was used, with the carbon electrodes
369 were placed 43 mm apart. The field strength used in these experiments was 350 V/m, with the polarity of
370 the electric field switching every 100 s. To allow for as many waveguides to be captured on the CCD
371 camera as possible, the electric field was turned off for 60 s after an actuation was complete. This
372 allowed the lattice to stay within the field of view of the camera, allowing the beam output to be captured
373 consistently over the course of the experiment. The intensity and position of each waveguide were
374 tracked using Trackpy (see **Supplementary Information S4**).

375 **Unidirectional remote actuation of cylindrical hydrogel waveguides**

376 We 3D printed a square prism cage (44 x 44 x 25 mm) with 4 electrode holders on each edge.
377 We placed 2 rectangular glassy carbon electrodes (25 x 25 x 3 mm) parallel to each other (**Figure S3a**).
378 The cylindrical hydrogel (diameter = 2 mm, L= 12 mm) was inserted through circular holes in the bottom of
379 the cage. The cage was sealed with a coverslip glued to the bottom. Waveguides were immersed in
380 buffer solution to a depth of 8 mm. These experiments were performed using individual cylinders, 2x2
381 arrays (4 waveguides) and 3x3 arrays (9 waveguides) of waveguides. The cylinders were illuminated with
382 a compact laser module (Thorlabs, USB Connector, $\lambda = 520$ nm, 0.9 mW) in conjunction with a beam
383 expander, placed underneath the cage housing the cylindrical waveguides. The time evolution of the
384 waveguide position was followed with a Moticam 3+ camera (1600 pixels (H) x 1200 pixels (V), Motic,
385 Hong Kong). The polarity of the electric field was switched every 180 s. The electric field was turned off
386 for 60 s, after which the electric field was inverted. This allows cylinders light intensity output to reach a
387 steady, nonchanging value. The position of the end of the waveguide as well as the intensity of the beam
388 output were analyzed using ImageJ.⁴³ The normalized intensity of individual waveguides was compared
389 to the calculated bending angles.

390 **Multidirectional bending of arrays of cylindrical waveguides**

391 To achieve multidirectional bending of individual cylindrical waveguides, we combined electric
392 fields generated from two power supplies connected to four glassy carbon plates (**Figure S3a**). Imaginary
393 lines traced along the direction of the electric field generated by each power supply were treated like an
394 axis. An example of the vectorial analysis carried out to combine the electric fields is shown in **Figure S3**.

395 The voltages employed to achieve each target angle as well as the polarity configurations on the carbon
396 plates are shown in **Figure 5a**. For the initial direction, the electric field was applied for 240 s, after which
397 the electric field was applied for 180 s. This process was repeated until the waveguide completed a full
398 cycle. It was assumed that the length of the cylinders remained 10 mm during the whole experiment. This
399 same procedure for multidirectional bending was used for the 2x2 and 3x3 arrays.

400 **Structural characterization of prisms with micro-channel waveguides**

401 A transmission microscope (Olympus BH2-UMA, Upright) coupled with a Moticam 3+ camera
402 was used to acquire micrographs of the channel waveguides at the entrance and exit face of the prisms.

403 **References**

- 404 1. *Learning from Nature how to Design New Implantable Biomaterials*. (Kluwer Academic Publishers,
405 2004).
- 406 2. Baker, L. J. *et al.* Diverse deep-sea anglerfishes share a genetically reduced luminous symbiont
407 that is acquired from the environment. *Elife* **8**, 1–21 (2019).
- 408 3. Ludt, W. B. & Clardy, T. R. First detection of biofluorescence in a deep-sea anglerfish. *J Fish Biol*
409 **100**, 843–846 (2022).
- 410 4. Bell, G. R. R. *et al.* Chromatophore radial muscle fibers anchor in flexible squid skin. *Invertebrate*
411 *Biology* **132**, 120–132 (2013).
- 412 5. Kuenstler, A. S., Kim, H. & Hayward, R. C. Liquid Crystal Elastomer Waveguide Actuators.
413 *Advanced Materials* **31**, 1–7 (2019).
- 414 6. Cheng, J. *et al.* Flexible Multifunctional Photonic Crystal Fibers with Shape Memory Capability for
415 Optical Waveguides and Electrical Sensors. *Ind Eng Chem Res* **60**, 8442–8450 (2021).
- 416 7. Kim, Y., Parada, G. A., Liu, S. & Zhao, X. Ferromagnetic soft continuum robots. *Sci Robot* **4**, 1–15
417 (2019).
- 418 8. Liu, L. *et al.* Light Tracking and Light Guiding Fiber Arrays by Adjusting the Location of
419 Photoresponsive Azobenzene in Liquid Crystal Networks. *Adv Opt Mater* **8**, 1–7 (2020).

- 420 9. Li, S. *et al.* Digital light processing of liquid crystal elastomers for self-sensing artificial muscles.
421 *Sci Adv* **7**, 3677–3700 (2021).
- 422 10. Regehly, M. *et al.* Xolography for linear volumetric 3D printing. *Nature* **588**, 620–624 (2020).
- 423 11. de Beer, M. P. *et al.* Rapid, continuous additive manufacturing by volumetric polymerization
424 inhibition patterning. *Sci Adv* **5**, 1–9 (2019).
- 425 12. Asvany, O., Yamada, K. M. T., Brünken, S., Potapov, A. & Schlemmer, S. Experimental ground-
426 state combination differences of CH₅⁺. *Science (1979)* **347**, 1346–1348 (2015).
- 427 13. Walker, D. A., Hedrick, J. L. & Mirkin, C. A. Rapid, large-volume, thermally controlled 3D printing
428 using a mobile liquid interface. *Science (1979)* **366**, 1–5 (2019).
- 429 14. Loterie, D., Delrot, P. & Moser, C. High-resolution tomographic volumetric additive manufacturing.
430 *Nat Commun* **11**, 1–6 (2020).
- 431 15. Kelly, B. E. *et al.* Volumetric additive manufacturing via tomographic reconstruction. *Science*
432 *(1979)* **363**, 1–6 (2019).
- 433 16. Dolinski, N. D. *et al.* Solution Mask Liquid Lithography (SMaLL) for One-Step, Multimaterial 3D
434 Printing. *Advanced Materials* **30**, (2018).
- 435 17. Basker, D. K., Cortes, O. A. H., Brook, M. A. & Saravanamuttu, K. 3D Nonlinear Inscription of
436 Complex Microcomponents (3D NSCRIPT): Printing Functional Dielectric and Metallodielectric
437 Polymer Structures with Nonlinear Waves of Blue LED Light. *Adv Mater Technol* **2**, 1–7 (2017).
- 438 18. Biria, S., Morim, D. R., Tsao, F. A., Saravanamuttu, K. & Hosein, I. D. Coupling nonlinear optical
439 waves to photoreactive and phase-separating soft matter: Current status and perspectives. *Chaos*
440 **27**, 1–21 (2017).
- 441 19. Hudson, A. D., Bacus, C., Whinton, M., Brook, M. A. & Saravanamuttu, K. Single-Step Generation
442 of Flexible, Free-Standing Arrays of Multimode Cylindrical Waveguides. *Adv Eng Mater* **21**, (2019).
- 443 20. Lin, H., Benincasa, K. A., Fradin, C. & Saravanamuttu, K. Shaping LED Beams with Radially
444 Distributed Waveguide-Encoded Lattices. *Adv Opt Mater* **7**, 1–9 (2019).

- 445 21. Lin, H., Hosein, I. D., Benincasa, K. A. & Saravanamuttu, K. A Slim Polymer Film with a Seamless
446 Panoramic Field of View: The Radially Distributed Waveguide Encoded Lattice (RDWEL). *Adv Opt*
447 *Mater* **7**, 32333–32345 (2019).
- 448 22. Hosein, I. D. *et al.* Waveguide Encoded Lattices (WELs): Slim Polymer Films with Panoramic
449 Fields of View (FOV) and Multiple Imaging Functionality. *Adv Funct Mater* **27**, (2017).
- 450 23. Feng, J. *et al.* Printed Degradable Optical Waveguides for Guiding Light into Tissue. *Adv Funct*
451 *Mater* **30**, 1–14 (2020).
- 452 24. Feng, J., Jiang, Q., Rogin, P., De Oliveira, P. W. & Del Campo, A. Printed Soft Optical
453 Waveguides of PLA Copolymers for Guiding Light into Tissue. *ACS Appl Mater Interfaces* **12**,
454 20287–20294 (2020).
- 455 25. Zhao, H., O'brien, K., Li, S. & Shepherd, R. F. Optoelectronically innervated soft prosthetic hand
456 via stretchable optical waveguides. *Sci Robot* **1**, 1–10 (2016).
- 457 26. Ramuz, M., Tee, B. C. K., Tok, J. B. H. & Bao, Z. Transparent, optical, pressure-sensitive artificial
458 skin for large-area stretchable electronics. *Advanced Materials* **24**, 3223–3227 (2012).
- 459 27. Missinne, J. *et al.* Stretchable optical waveguides. *Opt Express* **22**, 4168 (2014).
- 460 28. Van Meerbeek, I. M., De Sa, C. M. & Shepherd, R. F. Soft optoelectronic sensory foams with
461 proprioception. *Sci Robot* **3**, 1–7 (2018).
- 462 29. York, P. A., Kent, D. & Wood, R. J. Microrobotic laser steering for minimally invasive surgery. *Sci*
463 *Robot* **6**, 1–12 (2021).
- 464 30. Ma, H., Jen, A. K. Y. & Dalton, L. R. Polymer-based optical waveguides: Materials, processing,
465 and devices. *Advanced Materials* **14**, 1339–1365 (2002).
- 466 31. Han, D. *et al.* Soft Robotic Manipulation and Locomotion with a 3D Printed Electroactive Hydrogel.
467 *ACS Appl Mater Interfaces* **10**, 17512–17518 (2018).
- 468 32. Morales, D., Palleau, E., Dickey, M. D. & Velev, O. D. Electro-actuated hydrogel walkers with dual
469 responsive legs. *Soft Matter* **10**, 1337–1348 (2014).

- 470 33. Migliorini, L., Santaniello, T., Yan, Y., Lenardi, C. & Milani, P. Low-voltage electrically driven
471 homeostatic hydrogel-based actuators for underwater soft robotics. *Sens Actuators B Chem* **228**,
472 758–766 (2016).
- 473 34. Jin, S. *et al.* Preparation and electrical sensitive behavior of poly (N-vinylpyrrolidone- co-acrylic
474 acid) hydrogel with flexible chain nature. *Eur Polym J* **49**, 1871–1880 (2013).
- 475 35. Li, Y. *et al.* Electric Field Actuation of Tough Electroactive Hydrogels Cross-Linked by Functional
476 Triblock Copolymer Micelles. *ACS Appl Mater Interfaces* **8**, 26326–26331 (2016).
- 477 36. Duan, X. *et al.* Large-scale spinning approach to engineering knittable hydrogel fiber for soft
478 robots. *ACS Nano* **14**, 14929–14938 (2020).
- 479 37. Kim, S. J., Pugal, D., Wong, J., Kim, K. J. & Yim, W. A bio-inspired multi degree of freedom
480 actuator based on a novel cylindrical ionic polymer-metal composite material. *Rob Auton Syst* **62**,
481 53–60 (2014).
- 482 38. Wang, Y., Liu, J., Zhu, D. & Chen, H. Active tube-shaped actuator with embedded square rod-
483 shaped ionic polymer-metal composites for robotic-assisted manipulation. *Appl Bionics Biomech*
484 **2018**, (2018).
- 485 39. Burgess, I. B., Ponte, M. R. & Saravanamuttu, K. Spontaneous formation of 3-D optical and
486 structural lattices from two orthogonal and mutually incoherent beams of white light propagating in
487 a photopolymerisable material. *J Mater Chem* **18**, 4133–4139 (2008).
- 488 40. Allan, D. B., Caswell, T., Keim, N. C., van der Wel, C. M. & Verweij, R. W. soft-matter/trackpy:
489 Trackpy v0.5.0. (2021) doi:10.5281/ZENODO.4682814.
- 490 41. Hua, M. *et al.* 4D Printable Tough and Thermoresponsive Hydrogels. *ACS Appl Mater Interfaces*
491 **13**, 12689–12697 (2021).
- 492 42. Yao, Y. *et al.* Multiresponsive polymeric microstructures with encoded predetermined and self-
493 regulated deformability. *Proc Natl Acad Sci U S A* **115**, 12950–12955 (2018).
- 494 43. Schneider, C. A., Rasband, W. S. & Eliceiri, K. W. NIH Image to ImageJ: 25 years of image
495 analysis. *Nat Methods* **9**, 671–675 (2012).

